RESEARCH ARTICLE | MARCH 10 2023

Droplet-induced optical effects in an opto-microfluidic cross-configuration system

Leonardo Zanini ; Cinzia Sada

Physics of Fluids 35, 032007 (2023)
https://doi.org/10.1063/5.0138475

Physics of Fluids ARTICLE scitation.org/journal/phf

Droplet-induced optical effects in an opto-microfluidic cross-configuration system

Cite as: Phys. Fluids **35**, 032007 (2023); doi: 10.1063/5.0138475
Submitted: 12 December 2022 · Accepted: 18 February 2023 ·
Published Online: 10 March 2023

Leonardo Zanini[a] and Cinzia Sada[b]

AFFILIATIONS

Physics and Astronomy Department, University of Padova, Via Marzolo 8, 35131 Padova, Italy

[a]Electronic mail: leonardo.zanini.2@phd.unipd.it
[b]Author to whom correspondence should be addressed: cinzia.sada@unipd.it

ABSTRACT

A comprehensive description of all the optical phenomena occurring when light interacts with a moving dispersed phase in a constrained environment such as a real microfluidic channel is needed to perform a quantitative analysis as well as predictive one. This requires identifying fingerprints in the detected optical signal that are doubtlessly correlated with the shape and content type of the dispersed phase from those connected to uncertainties of the optical detection systems and/or instabilities in the microfluidics apparatus leading to dispersed phase size distribution. This article aims to model all the droplet-induced optical effects in an opto-microfluidic cross-configuration system and quantify how diffraction, transmission, absorbance, and reflection contribute to the overall response in the detected intensity after light-matter interaction. The model has been tested in the case of water droplets dispersed in hexadecane continuous phase as generated in an opto-microfluidic platform where optical waveguides are fully integrated with the microfluidic channels, so that light illuminates the flowing droplets from the channel wall and collected on the opposite side. A critical discussion of the impact of geometry and constrains is proposed as well as the impact of each contribute in terms of fingerprints in the detected signal. The good agreement obtained demonstrates the potentialities of both the derived model and the cross-configuration, getting information on droplet characteristics from the intensity arising from its light interaction.

I. INTRODUCTION

Optical diagnostics of flowing particles represents a valid and flexible investigation tool to determine the size, velocity, and number density of particles in a flow, with applications in particle sizing and detection of small amounts of outliers.[1,2] Most of the optical diagnostics approaches are based on illuminating a stream of particles and detecting the relative transmission of absorbance.[3] When light illumination of individual particles in the stream of dilute liquid suspension is achieved, a shadow or blockage of light results on the detector providing the so-called Single-Particle Optical Sensing (SPOS, also known as Light Obscuration, LO).[4] By measuring the reduction in the transmitted light intensity and using a calibration curve, it is possible to process the detector signal to determine the size of the particle. SPOS has gained increasing interest, thanks to the exploitation of laser-based systems as light illumination source[5] since miniaturization as well as optical characterization of particles can be carried out, including temperature, concentration, shape with direct application in fluid mechanics, such as analytic tasks, cytometry, reaction, and cooling crystallization systems, and dynamic light scattering.[5] SPOS has been widely employed in many fields, spanning from pharmaceuticals[6] to hydraulic/lubrication applications. Several theoretical studies have been, therefore, published on the light scattering, including refraction and transmission of particles depending on the shape (spherical or not) as well as composition, mostly focused on static geometries. In the last two decades, microfluidics has gained increasing attention in the field of optical sensing of pL and nL dispersed phases such as flowing particles and droplets, especially when combined with integrated optics to achieve opto-microfluidic platforms. The main aim is, in fact, to develop compact and portable devices with high sensitivity and low detection limits although using the lowest amount of sampled material possible. In order to achieve this result, several solutions have been proposed including fiber coupling to the microfluidic circuit even in hybrid solutions[7,8] as well as optical waveguides and microfluidics made by laser writing of SiO_2.[9–12] More recently, Ti in-diffused channel waveguides integrated to microfluidic channels by dicing have been made in $LiNbO_3$ as well.[13–15] In the last case, droplet velocity and refractive index sensors as well as protein detection have been demonstrated. When quantification analyses are considered, it is mandatory

to distinguish in the detected signal the contributes coming from: (i) the dispersed phase content to be quantified; (ii) artifacts coming from imprecisions and/or inaccuracies in the microfluidics setup that impact on the dispersed phase generation widening the size distribution of the dispersed phase; (iii) instabilities in the optical signal coupling/detection analysis. Independently of the fabrication technology, in fact, one of the key factors is the reproducibility of the signals labeling the dispersed phase and, consequently, the capability to identify the fingerprints that are truly connected with the species to be quantified. As a consequence, in order to get SPOS be fully informative, modeling of the optical response is needed. Although the optical properties of such particles have been studied since the beginning of the last century with Mie and even more in detail in the fifties,[16] light scattering for optical particle sizing was started to be deeply investigated later,[17–20] including the scattering of an arbitrary shaped beam by a multilayered sphere,[21] the description of distortions of Single-Particle Optical Sensing (SPOS) Particle Count by Sub-Countable Particles[22] up to *In situ* particle sizing.[23] Very recently, applications to microfluidics have been reported with measurements and modeling of dynamic light scattering (DLS) of fiber for measuring the distribution of the size of particles in a microfluidic chip[24–26] as well as the optical microparticle size detection by phase-generated carrier demodulation.[27] Light scattering properties of large spherical bubbles have been recently described from a theoretical point of view by using geometrical and physical optics approximations,[28] with ray tracing advanced techniques and Monte Carlo simulations[29] applied to colloidal suspensions. Interference occurring between higher-order rays, the Goos–Hänchen shift, the tunneling phase, and the weak caustic associated with the critical angle was considered to characterize the optical response of bubbly flows, in agreement with the scattering diagrams predicted by the Lorenz–Mie theory (LMT). Calculations of the near-field power inside and outside an air bubble in water of radius lower than few μm in the visible range have been proposed and then applied to colloid suspension droplets because of their great interest in many industrial processes, including fuels, pharmaceutical applications as well as agricultural and domestic sprays. Although several applications to colloidal suspensions have been published, colloid inclusions were assumed uniform in size and spherical in shape, in dilute concentration so that to assume the Lambert Beer law be valid. In several cases, the Mueller matrix was used to calculate the Stokes vector for the reflected light ray and transmitted light ray,[30] and the total internal reflection accurately computed to identify signal characteristics which may be used to estimate the colloidal concentration from individual droplets, in addition to their size and velocity (see Ref. 29 and reference therein quoted). A model of light interaction that considers the dispersed phase environment, including the role of the continuous phase they are immersed in, is still lacking. The effect of boundary conditions such as those due to a microfluidic channel and its geometry as well as the effect of illumination made by optical waveguides or fibers integrated with the microfluidic channel to form one portable opto-microfluidic platform is of primary importance.

As a matter of fact, despite the great impact of these techniques and significant importance of the description of the physical phenomena behind with a wide spectrum of application benefitting of their application, in most cases, randomly distributed particles or single individual spherical particles have been modeled, immersed in a homogenous medium that neither does interact nor provides a direct contribute to the optical response of the flowing particle a part eventual optical refractive index contrast. A comprehensive description of all the optical phenomena occurring when light interacts with a moving dispersed phase in a constrained environment such as a real microfluidic channel is needed to identify fingerprints in the detected optical signal that are doubtlessly correlated with the shape and content type of the dispersed phase from those connected uncertainties of the optical detection systems and/or instabilities in the microfluidics apparatus leading to dispersed phase size distribution.

This article aims to contribute in covering these gaps and reports the modeling of droplet-induced optical effects in an opto-microfluidic cross-configuration system. The case study of this work is a device in which a microchannel and a waveguide are integrated on the same monolithic substrate to cross each other perpendicularly, with the former splitting the latter into two collinear guides facing onto the channel. The waveguides are obtained close to the substrate surface, therefore illuminating the channel from the top of the lateral wall, while a cover is glued onto the substrate to achieve a closed and compact device. Particularly, this paper describes in detail the mathematical modeling of the light interaction between a droplet flowing in the channel and a waveguide illuminated from its input and acting as a light source (in the following, input waveguide). By construction, the light resulting from the interaction is collected by the opposite collinear waveguide (output waveguide) and brought away from the channel for acquisition. Moreover, in this work, a reference device in $LiNbO_3$ has been realized according to Refs. 14 and 31, reproducing the same configuration of Fig. 1(a). In the latter, several waveguides are spaced and integrated in the reported configuration. The successful comparison of the theoretical expectations with real data acquired through the reference device is discussed in the following, showing the great potentiality of the model prediction.

The general approach used in modeling the light interaction with a droplet as exposed in this work can be readapted for other similar devices without being limited to the reference chip in $LiNbO_3$ herein considered. Moreover, while we are focusing on the light interaction with droplets due to their various applications in microfluidics,[32,33] the working principle of the modeling here presented can be readjusted and applied also to other flowing objects (like cells) without losing validity. This aspect gives a boost in the investigation proposed since the popularity of similar opto-microfluidic cross-configurations, enabling quick analyses of the optical response of flowing specimens.

In the presented configuration, the droplet while crossing the light source can be considered a moving obstacle providing diffraction, transmission, absorbance, and reflection. Each phenomenon contributes differently, and the overall response is a convolution of all these effects. Some of them are mostly dependent on the interface shape (refraction), and others on the medium (absorbance) or on the confinement of the droplet within a channel (diffraction). In the literature, some investigations have been proposed to describe droplets flowing in cylindrical microfluidic channels.[34–37] In that case, despite being only theoretical, the system symmetry strongly simplified the analytical solution of the problem. In this work, instead, we analyze a real case of droplets flowing in a rectangular closed microfluidic channel, illuminated by an integrated optical waveguide obtained on the top of the lateral wall and perpendicular to the microfluidic channel itself.

In order to model the light interaction with moving droplets, a frame-to-frame approach has been employed, picturing each optical

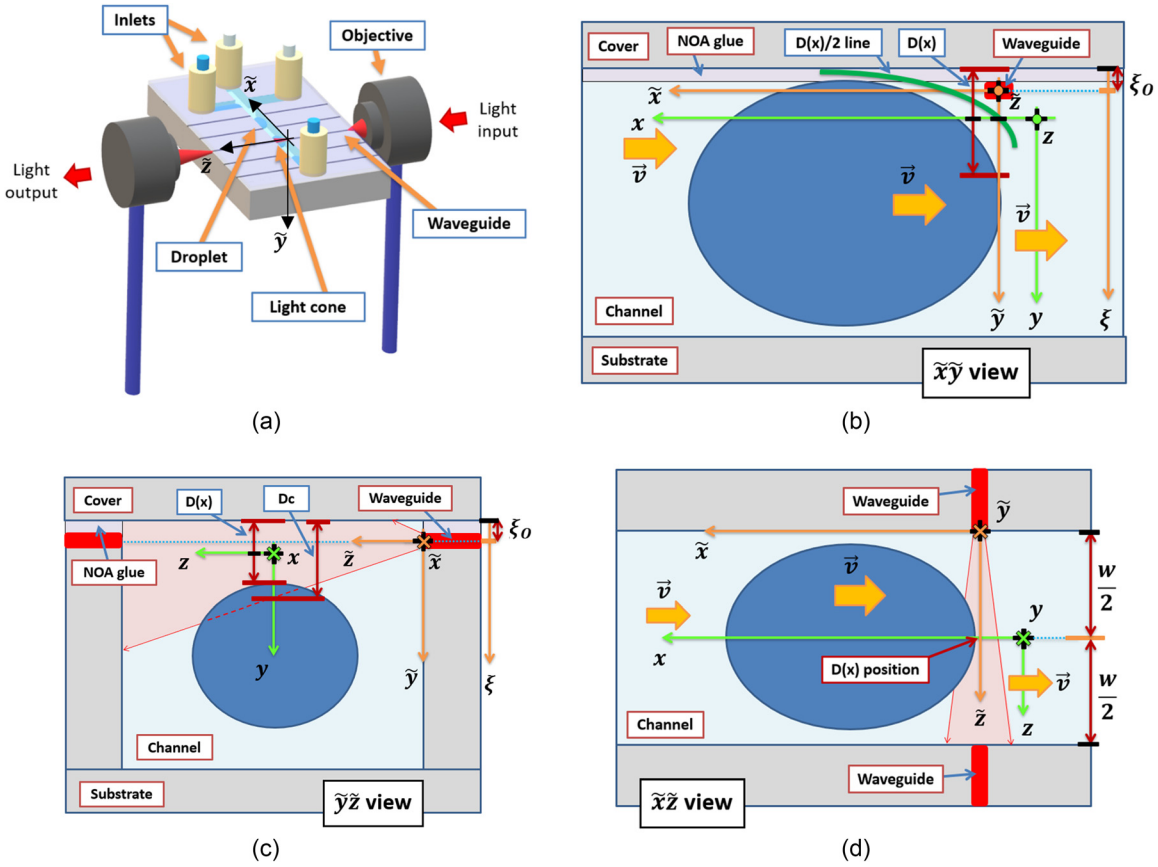

FIG. 1. (a) Scheme of the opto-microfluidic platform with the coordinate system $\tilde{x}\tilde{y}\tilde{z}$ fixed with the waveguide. Water droplets (in blue) are flowing in the microchannel as surrounded by the hexadecane (in light blue). Figures (b)–(d) report the sections of the system along, respectively, the planes $\tilde{x}\tilde{y}$ (at the middle of the channel), $\tilde{y}\tilde{z}$ (at the waveguide position), and $\tilde{x}\tilde{z}$ (at the waveguide height). The droplet reference system xyz is also reported in (b)–(d) together with the distance $D(x)$ between the cover bottom and the droplet top precisely in front of the waveguide. The vertical coordinate ξ is reported only in (b) and (c). The red rectangles depicted in (b)–(d) are the related sections of the optical waveguide. The microchannel width is indicated in (d) as w (in the reference device 200 μm). The green line in (b) represents the locus of points corresponding to the center of the distance $D(x)$.

effect (OE_i, i = refraction, transmission, absorbance, diffraction, etc.) in a given position of the flowing droplet and calculating the related optical response (OR_i) by using the proper reference system when necessary. The light intensity detected at the output waveguide can be, therefore, expressed in terms of a sum of all the optical responses OR_i induced in that given position of the droplet. Since the droplet is flowing, this sum and its components OR_i are functions in time of the droplet changing position. To include the latter in the model, the strategy adopted is to express this time dependence in the OR_i through a common geometrical parameter linked to the droplet flow. Looking at the sections of the interacting system, as reported in Figs. 1(b) and 1(c), it emerges that the optical interaction strongly depends on the distance between the device covering bottom and the droplet covering top in front of the waveguide. In fact, this distance—defined as D—determines whether the droplet covers the collecting guide, boosting the transmission inside the droplet, or not, resulting in the predominance of other effects. Moreover, since D changes in time accordingly with the droplet motion, its variation in time $D(t)$ reproduces the longitudinal profile of the droplet moving inside the microfluidic channel, carrying the information on its shape. In general, $D(t)$ depends on the microfluidic experimental conditions, for example, the ratio of the flows of the continuous and dispersed immiscible phases mixed to form droplets in T-junction or Cross-junction configurations, respectively. As a consequence, $D(t)$ has been considered the most suitable parameter for a unitary description of all the OR_i linked to the droplet motion and shape. This implies to limit the calculation to a 2D system, as reported in Figs. 1(c) and 2, considering the section of the system at the waveguide position. Once all the responses are reported as functions of $D(t)$, the time pattern of the intensity $I(t)$ collected during the droplet transit is directly obtained from the calculated sum by inserting the time expression of $D(t)$. Since it is much more intuitive to work with the droplet profile in the space, directly expressing it in terms of the longitudinal coordinate of the channel, in this work, we introduced this profile by expressing $D(t)$ in a reference system xyz [see Fig. 1(b)] moving together with the droplet along the microchannel parallel to its x-axis. In this frame, $D(t)$ is turned into a spatial dependence on x as $D(x)$, with x the waveguide position in the moving frame xyz, linear in t via the droplet velocity. This also turns the

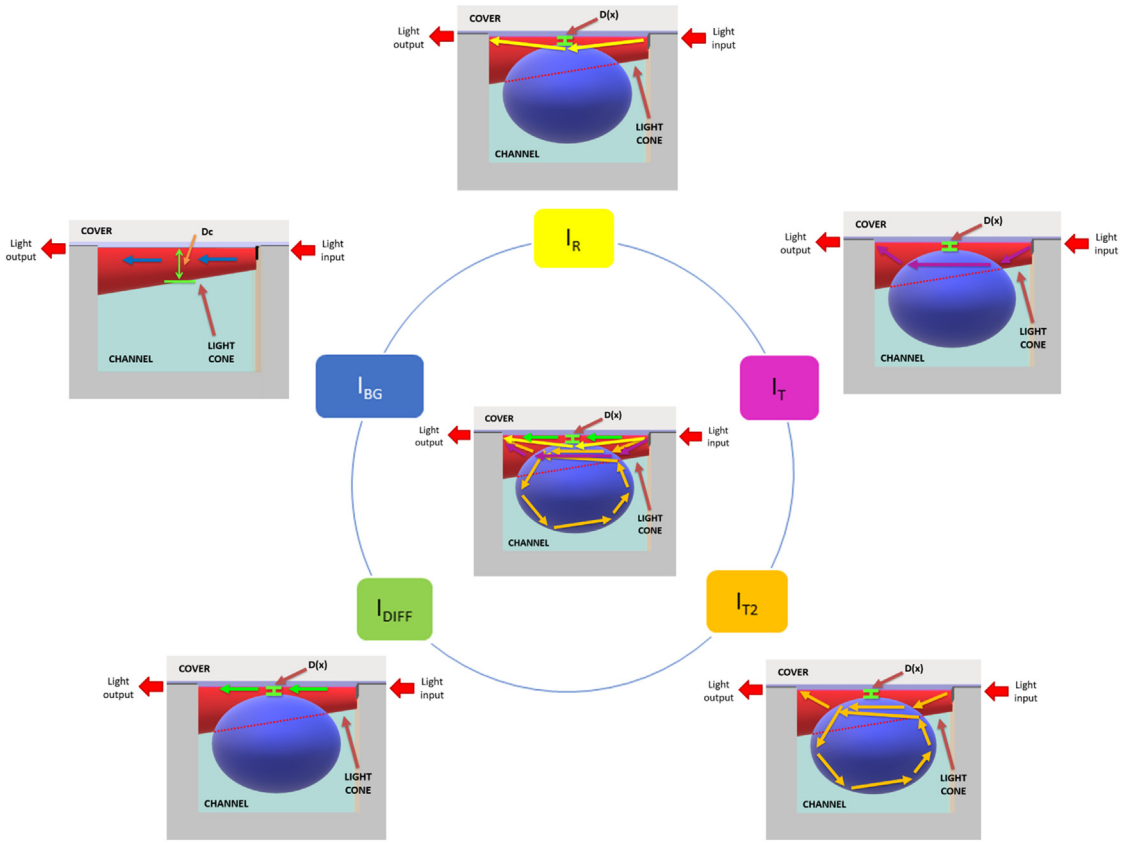

FIG. 2. Contributes to $I(x)$: background, reflection, transmission, and diffraction. Sections along the plane $\tilde{y}\tilde{z}$ (at the waveguide position) in the waveguide frame are depicted with schemes of the light rays.

intensity pattern $I(t)$ into a spatial dependence on the same x as $I(x)$, directly linked to the droplet longitudinal profile expressed by $D(x)$ and comparable with the time dependent experimental signals due to the linearity between x and t.

In Sec. II, all the main optical responses are quantified separately through this approach as functions of $D(x)$ and x in the droplet reference system. The explicit calculation of each contribute is detailed in the supplementary material. The convolution effect resulting from their interplay is then estimated, providing an expression of $I(x)$ at the output waveguide, where all the correlations with the droplet characteristics in shape and content are evidenced. The model is then applied to a real case study to show its performances and potentialities by simulating the responses of the $LiNbO_3$ reference device for droplets with different shapes. These theoretical predictions are also successfully compared with experimental results acquired on droplets of comparable shape and same content through the real reference device in $LiNbO_3$.

II. THE MODEL: LIGHT INTERACTION WITH THE DROPLET

As reported in Fig. 1(a), two reference systems have been used to estimate the light intensity detected at the output waveguide:

- the waveguide reference system $\tilde{x}\tilde{y}\tilde{z}$, time independent, with origin in the center of the input waveguide in the channel and axes as depicted in Fig. 1;
- the droplet reference system xyz, with the axes x, y, and z parallel, respectively, to the axes $\tilde{x}$, $\tilde{y}$, and $\tilde{z}$, with the origin of the x-axis moving together with the droplet, z-axis fixed at the channel center and of the y-axis placed at the center of the distance $D(x)$ in front of the waveguide as the droplet is moving [following the green line in Fig. 1(b)].

The model assumes that the droplet center moves along the x direction. Auxiliary variables have been introduced to simplify the calculations when useful (see supplementary material for further details). In the droplet frame xyz, $I(x)$ is given by the sum of several contributes $I_i(x)$ as sketched in Fig. 2:

- I_R,light reflected from the droplet top;
- I_T, light transmitted by the droplet, even after an internal reflection inside the droplet $I_{T,FC}$;
- I_{T2}, light transmitted after several internal reflections inside the droplet;
- I_{DIFF}, light diffracted as the distance $D(x)$ in front of the waveguide acts as a slit;

- I_{BG}, light collected when the droplet does not intercept the light cone, thus representing a background.

In this work, each term $I_i(x)$ has been obtained from the calculated optical responses $OR_i(x)$ expressed in terms of $D(x)$ at the given position x. Each calculated optical response $OR_i(x)$ is weighted by a specific step function $f_i(x)$ that depends on the optical phenomenon under consideration (refraction, transmission, absorbance, diffraction, etc.) and dynamically switches $OR_i(x)$ on/off based on its real impact. The full expression of $I(x)$ is, therefore, given by

$$I(x) = \sum_i I_i(x) = \sum_i f_i(x) OR_i(x). \tag{1}$$

The approach is general and can be applied to any type of dispersed/continuous phases combination. In order to verify the model prediction, a dispersed phase with lower refractive index with respect to the continuous case has been considered, so that experimental data with water droplets surrounded by hexadecane oil can be used as a real case study for comparison.

A. Contribute of diffraction: I_{DIFF}

When the droplet intersects the input waveguide, a diffractive pattern is detected at the output waveguide because the droplet behaves as an obstacle. This phenomenon has been modeled assuming the droplet as an opaque medium that creates a slit of width equal to $D(x)$. According to Fig. 1(c), such diffractive phenomenon occurs only when $D(x) < D_C$, where D_C represents a threshold value that can be estimated as

$$D_C = \frac{w \cdot NA}{2n_o} + \xi_0$$

corresponding in Fig. 1(c) to the maximum value of $D(x)$, for which the droplet top intercepts the beam at the channel center. The incident Electro-Magnetic (EM) field illuminating $D(x)$ has been calculated applying the Huygens–Fresnel principle in paraxial approximation and for a Gaussian profile exiting from the input waveguide. In the droplet frame xyz, it results that

$$E(x, y, z = 0) = E_O(w/2) e^{-\left(\frac{y-\xi_o+\frac{D(x)}{2}}{\frac{wNA}{2n_o}}\right)^2} e^{i\omega t} e^{-ik\left[\frac{\left(y-\xi_o+\frac{D(x)}{2}\right)^2}{w}+\frac{\phi\left(\frac{w}{2}\right)}{k}\right]}, \tag{2}$$

where w is the channel width, n_O is the continuous phase refractive index, $k = 2\pi n_O/\lambda$, $NA = n_o sen\theta_o$ is the numerical aperture, and $E_O(w/2)$ is the field amplitude at the middle of the channel. By integrating the previous equation along the slit over y ranging in $\left[-\frac{D(x)}{2}; \frac{D(x)}{2}\right]$ and including the corresponding phase factor as predicted by the Huygens–Fresnel principle, we have estimated $E(x)$ at $z = w/2$, i.e., at the collecting waveguide position. When y is high enough, the Fraunhofer approximation is not strictly valid, but, in this case, the term $e^{-iky^2/w}$ can be neglected. Moreover, for bigger droplets, i.e., when $D(x)$ is small enough, the term $e^{-\left(\frac{y-\xi_o+\frac{D(x)}{2}}{\frac{wNA}{2n_o}}\right)^2}$ can be approximated as a constant (effective) mean value $\overline{A}$, and a uniform field approximation can be applied with an accuracy of the 15%. Under these hypotheses, we can assume $E(x) \sim E(x)|_{unif}$ given by

$$E(x)|_{unif} := \frac{2n_O}{w\lambda} \int_{-D(x)/2}^{D(x)/2} \overline{A} e^{i\omega t} e^{-iky\frac{(D(x)/2-\xi_o)}{w/2}} dy$$

$$= \frac{2n_O}{w\lambda} \overline{A}\, D(x) e^{i\omega t} \frac{sen\left(\frac{n_O \pi D(x)}{\lambda}\left(\frac{D(x)/2-\xi_o}{w/2}\right)\right)}{\frac{n_O \pi D(x)}{\lambda}\left(\frac{D(x)/2-\xi_o}{w/2}\right)} \tag{3}$$

and, consequently, $OR(x)_{DIFF} \sim OR(x)_{DIFF|unif}$ given by the average $\left\langle \left| E(x)|_{unif} \right|^2 \right\rangle_t$ made over time. The intensity $I(x)_{DIFF}$ is expressed, therefore, as

$$I(x)_{DIFF} \sim f_{DIFF}(x) \cdot OR(x)_{DIFF|unif}, \tag{4}$$

where $f_{DIFF}(x)$ is the relative step function

$$f_{DIFF}(x) = 1 - \frac{1}{1 + c_1\left(\frac{D_C + c_3}{D(x)}\right)^{c_2}} \tag{5}$$

with c_1, c_2, and c_3 parameters ensuring a smooth transition and assuring to switch on this phenomenon effect only for $D(x) < D_C$. The final expression of $I(x)_{DIFF}$ is computed by expressing the constant $\overline{A}$ in Eq. (3) in terms of P the light power illuminating the channel and ω_o the beam waist (see supplementary material). The obtained result of $I(x)_{DIFF}$ shows that the droplet profile $D(x)$ acts as a unifying parameter in the optical description. Particularly, this implies that the resulting modeled signal always shows similar behaviors in the presence of specific values of $D(x)$, despite considering different droplet profiles. For example, from Eq. (3), $I(x)_{DIFF}$ is predicted to have a maximum when $D(x)|_{\max} = 2\xi_0$ and minima when

$$D(x)_{\min} = \xi_0 + \sqrt{{\xi_0}^2 + m \cdot \lambda w/n_o},$$

where m is an integer number. For the case considered, since $\xi_0 \sim \mu$m, $\lambda w \sim 10^2 \mu$m, and $I(x)_{DIFF}$ are limited to $D(x) < D_C$, it results that $m = +1$, and only the first order of minima is detected.

B. Contribute of the background: I_{BG}

For $D(x) > D_C$, the droplet does not intercept the light cone exiting the guide. By using the same formalism of Sec. II A, the emitted power P is subdivided at the channel end in a circular area (see Fig. 1) with radius wNA/n_o. The optical response is then $OR(x)_{BG} = \frac{Pn_o^3}{\pi \cdot w^2 NA^2}$, for all x related to $D(x) > D_C$, and is modulated by a step function $f_{BG}(x) = \left[\frac{1}{1+d_1\left(\frac{D_C}{D(x)}\right)^{d_2}}\right]$, so that

$$I(x)_{BG} = \frac{Pn_o^3}{\pi \cdot w^2 NA^2} \cdot \left[\frac{1}{1 + d_1\left(\frac{D_C}{D(x)}\right)^{d_2}}\right], \tag{6}$$

where d_1 and d_2 are parameters ensuring a smooth transition.

C. Contribute of reflection from the droplet surface: I_R

The intensity I_R collected at the output waveguide generated by rays reflected at the droplet surface has been calculated using Snell's

law in function of the refractive index of the continuous phase (n_O) and the dispersed one (n_d), as functions of the polarization and angle of incidence θ_{IN}. In the following, the case $n_O > n_d$ is considered, so that the model predictions can be compared to experimental data of water droplets surrounded by hexadecane as a case study. Under such situation, rays incident on the droplet surface at an angle greater than the critical angle θ_c undergo to Total Reflection (TIR). In this case, no transmission will occur inside the droplet. For water ($n_d = 1.33$) droplets immersed in a hexadecane ($n_O = 1.43$) continuous phase, θ_c is close to 68.44°.

In general, rays reflected at the interface are mostly dispersed in the channel without reaching the output guide. Instead, rays impinging exactly on the droplet top are reflected and coupled by symmetry into the output waveguide, as shown in Fig. 2 in correspondence of I_R. On the droplet top, the incidence angle θ_{IN} with respect to the surface normal is calculated in the special case of $D(x) = D_C$ and $z = 0$ resulting in

$$\theta_{IN} = arctg\left[\frac{w/2}{D_C - \xi_0}\right] = arctg\left[\frac{n_o}{NA}\right] > \theta_c, \tag{7}$$

i.e., TIR occurs. By geometry, Eq. (7) is verified also for $\forall D(x) < D_C$ because $\theta_{IN}(D_C) < \theta_{IN}(D(x))$. This phenomenon contributes to the light intensity detected at the output waveguide with an additional term $I(x)_R$. Reflection from the top of the droplet starts to be detected when the droplet enters in the light cone ($D(x) \approx D_C$) and stops when $D(x) \leq \xi_0$. As a consequence, a suitable step function is

$$f_R(x) = \frac{1}{1 + a_1\left(\frac{\xi_0 + a_2}{D(x)}\right)^{a_3}}, \tag{8}$$

where a_1, a_2, and a_3 are parameters ensuring a smooth transition between the two regimes. Finally, $OR_R(x)$ is estimated using Eq. (2) for calculating the intensity incident on the droplet top at the channel center. Under these hypotheses, it can be derived (see supplementary material for details) that $I(x)_R$ results

$$I(x)_R = f_R(x) \cdot \frac{4Pn_o^3}{\pi \cdot w^2 NA^2} \cdot \rho \cdot e^{-2\left(\frac{D(x)-\xi_0}{(wNA/2n_0)}\right)^2} =: f_R(x) \cdot OR_R(x), \tag{9}$$

where $\rho = 2\sqrt{\frac{2}{\pi}} \cdot \frac{1}{0.9545}$ has been calculated in the supplementary material.

On the other hand, the rays impinging on the droplet surface before the droplet top at an incidence angle greater than θ_c directly affect the modeling of the diffraction, since they increase the light intensity crossing the slit between the top of the droplet and the microfluidic cover. As a consequence, a correction factor $\delta(x)$ has been, therefore, included in Eq. (4) in order to account for this effect that produces a sort of light collimation,

$$\delta(x) = 1 + \alpha_C\left[\left(\frac{D_C}{D(x)}\right)^2 - 1\right] \cdot \left[\frac{1}{1 + \left(\frac{\xi_0 + b_1}{D(x)}\right)^{b_2}}\right] \cdot \left[1 - \frac{1}{1 + \left(\frac{D_C}{D(x)}\right)^{b_3}}\right], \tag{10}$$

where b_1, b_2, and b_3 are parameters. As a consequence, Eq. (4) is turned into

$$I(x)_{DIFF} = f_{DIFF}(x) \cdot \delta(x) \cdot OR_{DIFF}(x). \tag{11}$$

D. Contribute of transmission through the droplet

Three main contributes to the light transmission after the light-droplet interaction have been considered:

- I_T—"direct" transmission without internal reflection inside the droplet [Fig. 3(a)];
- I_{T2}—transmission occurring after internal reflections ($R \neq 0$) have occurred inside the droplet [Fig. 3(b)];
- $I_{T,FC}$—transmission after one internal reflection ($R \neq 0$) has taken place inside the droplet on the bottom of the droplet top [Fig. 3(c)].

As far as I_T is considered, the transmittance across the droplet has been estimated depending on the angle of incidence using Snell's law. Moreover, since by construction, I_T is different from zero only when $D(x) \leq \xi_0$, a suitable step function $f_T(x)$ is therefore

$$f_T(x) = 1 - \frac{1}{1 + \left(\xi_0/D(x)\right)^{\alpha}} \rightarrow \begin{cases} 0 & if\ D(x) \gtrsim \xi_0, \\ 1 & if\ D(x) \lesssim \xi_0. \end{cases} \tag{12}$$

Introducing some approximations, such as locally neglecting the droplet curvature in the propagation of the transmitted rays, so that they all lay along the z-axis (see supplementary material), the optical response $OR_T(x)$ has been estimated by the ratio between the emitted power P from the input waveguide and the illuminated circular area at the output waveguide, resulting in

$$OR_T(x) = \frac{Pn_o}{\pi \cdot r^2} \cdot T_{t1}T_{t2} = \frac{Pn_o}{\pi \cdot \left(\frac{NA}{n_o}(w - z_D) + \frac{NA}{n_d}z_D\right)^2} \cdot T_{t1}T_{t2}, \tag{13}$$

where the transmittances at the two interfaces of the droplet met by the transmitted ray (T_{t1}, T_{t2}) have been included. In Eq. (13), z_D is the optical path inside the droplet (with refractive index n_d), while $(w - z_D)$ is the optical path outside it (with refractive index n_o). $I(x)_T$ is modeled as

$$I(x)_T = f_T(x) \cdot T_{t1}T_{t2} \frac{Pn_o}{\pi \cdot \left(\frac{NA}{n_o}(w - z_D) + \frac{NA}{n_d}z_D\right)^2} \cdot (1 - c_N\sigma z_D), \tag{14}$$

where $(1 - c_N\sigma z_D)$ is a correction factor counting for absorbance effects inside the droplet, assuming the Lambert–Beer law approximated for thin slices such as $z_D < 200\ \mu$m (where c_N is the concentration and σ is the extinction cross section of the dispersed absorbing centers in the droplet).

Focusing instead on the situation of Fig. 3(c), it can be easily deduced under the same approximations exploited for the calculation of I_T that this is the case of rays entering in the droplet with $D(x) \sim \xi_0$. In this geometrical configuration, after one internal reflection, the rays are transmitted outside the droplet, enhancing the

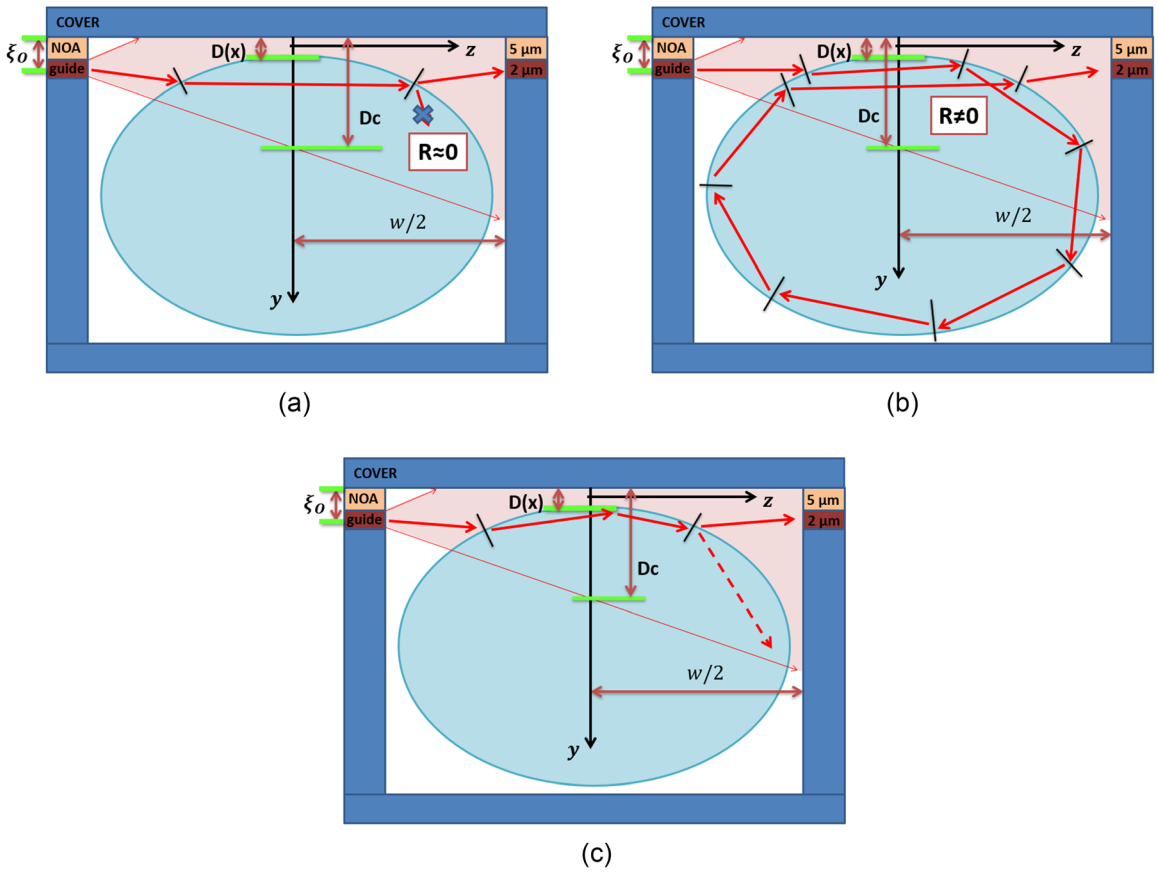

FIG. 3. Sketch of the light transmission mechanism in the droplet: (a) direct transmission, (b) transmission after several internal reflections, and (c) transmission after one internal reflection ($R \neq 0$) occurred inside the droplet.

intensity of light reaching the output waveguide. A further contribute has been included to quantify this effect: $I(x)_{T,FC}$ (FC = First Contact), modulated by a step function $f_{FC}(x)$. It can be demonstrated similarly as for I_T that

$$I(x)_{T,FC} = f_{FC}(x) \cdot R_{FC} T_{FC1} T_{FC2} \frac{Pn_o}{\pi} \cdot \left[\frac{1}{\left(\frac{NA}{n_o}(w - z_D) + \frac{NA}{n_d} z_D \right)^2} \right] \cdot G_i(x, \lambda) \cdot (1 - c_N \sigma z_D b_T) =: f_{FC}(x) \cdot OR_{FC}(x), \quad (15)$$

where T_{FC1} and T_{FC2} are the transmittances at these interfaces, R_{FC} is the relative reflectance coefficient, $(1 - c_N \sigma z_D b_T)$ is the absorbance, $(b_T z_D)$ is the optical path inside the droplet expressed in terms of z_D units, and $G_i(x, \lambda) = G_i\left(\sum_{i=0}^{m} e^{-\left(\frac{D(x) - \xi_0 + h_i'}{\beta} \right)^2} \right)$ is a factor that considers the number m of reflected rays as detailed in the supplementary material. Moreover, in this case, the step function $f_{FC}(x)$ is given by

$$f_{FC}(x) = 1 - \frac{1}{1 + \left(\xi_0 / D(x) \right)^{\alpha}} \rightarrow \begin{cases} 0 & if\ D(x) \gtrsim \xi_0, \\ 1 & if\ D(x) \lesssim \xi_0. \end{cases} \quad (16)$$

Finally, transmission from rays that have been internally reflected within the droplet has been estimated with a similar procedure exploited in the previous cases. In the simulation, a value between ξ_0 and D_C, $D(x) = 2\xi_0$, has been simulated as the critical slit width $D(x)$ for this phenomenon to happen. By applying Snell's law and considering the light reflected several times before exiting from the droplet, it can be demonstrated that

$$I(x)_{T2} = f_{T2}(x) \cdot T_{t3} T_{t4} \overline{R}_T \frac{Pn_o}{\pi} \cdot \frac{1}{\left(\frac{NA}{n_o}(w - z_D') + \frac{NA}{n_d} z_D' \right)^2} \cdot F_i(x, \lambda) \cdot (1 - c_N \sigma w l_T) =: f_{T2}(x) \cdot OR_{T2}(x), \quad (17)$$

where $\overline{R}_T$ is an average reflectivity considering the several internal reflections inside the droplet, z_D' is the path in the droplet before the first internal reflection occurs, T_{t3} and T_{t4} are the transmittances at the droplet interfaces (to enter the droplet and exit from it, respectively), $F_i(x, \lambda)$ is a factor that accounts for the fact that I_{T2} has contributed also for other rays incident at a depth lower than $2\xi_0$, and wl_T is the overall optical path. The suitable step function to switch I_{T2} on/off is, therefore, simulated as

$$f_{T2}(x) = 1 - \frac{1}{1 + \left(2\xi_0/D(x)\right)^{\alpha}} \rightarrow \begin{cases} 0 & \text{if } D(x) \gtrsim 2\xi_0, \\ 1 & \text{if } D(x) \lesssim 2\xi_0. \end{cases} \quad (18)$$

Considering the interplay between the direct and the diffused transmission, it emerges that the overall contribution from the light transmission to the light intensity detected at the output waveguide is equal to

$$I(x)_T + I(x)_{T2} \sim T_{t1}T_{t2} \cdot (1 - n\sigma z_D) + T_{t3}T_{t4}\overline{R}_T \cdot F_i(x) \cdot (1 - n\sigma w l_T) \quad (19)$$

and since $T_{t1}T_{t2} \ll T_{t3}T_{t4}\overline{R}_T \cdot F_i(x)$ then $(1 - n\sigma z_D) \gg (1 - n\sigma w l_T)$, with absorbance much more influenced by the term $I(x)_{T2}$, as expected by geometrical considerations.

E. Dynamics: Interplay of the optical phenomena

In order to define the role of each step function, the dynamics of the light interaction with the droplet has been considered. The following main situations occur:

1. when $D(x) > D_C$, no interaction occurs between the droplet and the light exiting from the input waveguide. In this case, the droplet is far away from crossing the optical waveguide, or the radius of the section along the yz plane is too small;
2. when $D(x) < D_C$, the droplet starts crossing the optical waveguide. Both diffraction from a slit of width $D(x)$ and TIR on the droplet top are observed;
3. if $\xi_0 < D(x) < D_C$, then TIR strongly contributes and I_{T2} increases;
4. when $D(x) \approx \xi_0$, being in axis with the waveguide, TIR becomes less effective and I_T is still not observed;
5. when $D(x) \leq \xi_0$, I_T starts to contribute significantly together with the remaining components I_{T2} and I_{DIFF}.

In addition, depending on the interplay of each contribute, different fingerprints appear in $I(x)$ that can be used as key indicators for optical sensing. In particular

(a) if the droplets content is to be investigated, the most convenient condition is $D(x) \leq \xi_0$ because both I_T and I_{T2} predominate. This means that the portion of the experimental signal to be used for concentration quantifications of the droplet content must be the part satisfying this condition;
(b) if the focus is on the droplets counting, then the best condition is given by $\xi_0 < D(x) < D_C$ because I_{DIFF} prevails. In this case, the ratio between the maximum of such peaks and $I(x)_{BG}$ is at least around 4, as shown in the next section, thus giving a boost in marking the droplet transit in the channel;
(c) to estimate the droplets size, the positions of the diffraction minima are the best indicators because it is possible to identify different dispersed phases or same dispersed but with different size distribution by monitoring the relative positions of I_{DIFF} minima.

III. RESULTS

Based on the modeling presented in Sec. III, $I(x)$ has been computed as a function of the droplet profile along the microchannel axis, $D(x)$, for a given wavelength λ and dispersed/continuous phases refractive indexes n_d and n_o. In order to test its prediction potentialities and validate the assumptions the model is based on, its parameters have been settled to reproduce a concrete case of droplets generated by a real opto-microfluidic platform, considering the reference case of a microchannel of width $w = 200\,\mu$m engraved in $LiNbO_3$ and covered by glass as in Ref. 31. In particular, an incident wavelength $\lambda = 632.8$ nm and water droplets ($n_d = 1.33$) dispersed in a continuous phase of hexadecane oil ($n_O = 1.43$) have been used. Moreover, the width and the height of the optical waveguides have been set to $2\,\mu$m, while the glue layer thickness between the cover and the substrate has been fixed to $5\,\mu$m in order to reproduce the experimental geometry of the real device, with $\xi_0 = 6\,\mu$m and $NA = 0.13$ (see Ref. 31 for further details on the experimental device and its performances). In this configuration, $D_C \approx 16\,\mu$m and droplets are considered big (i.e., filling almost the entire channel section) if $D(x) < 10\,\mu$m. Other parameters set in the simulation are $\rho \approx 1.67$, $F_i(x) \sim 5$, $\overline{R}_T = 0.1$, and $G_i(x) \approx 5$ (see supplementary material for details).

Based on the established geometry and depending on the microfluidic conditions, droplets can assume spherical and symmetrical shapes (dripping regime) up to long and asymmetrical ones (squeezing regime). In the following, three droplet profiles $D(x)$ have been chosen to represent three different microfluidic configurations with respect to the input waveguide, such as the squeezing and the dripping regimes and the transition between the two. In particular, two extreme cases have been studied herein: spherical droplets moving far away from the input waveguide (i.e., dripping far from the waveguide) and asymmetric droplets filling almost all the microfluidic channel (squeezing over the waveguide). It is worth mentioning that small droplets that do not cross the waveguide but intersect the light cone fulfilling the condition $D(x) < D_C$ as in Fig. 1(c) (like in the case of the dripping far from the waveguide) represent the detection limit of the device.

Experimental images of water droplets dispersed in hexadecane have been used to extract the experimental profile of $D(x)$, which is then parametrized with analytical solutions in order to check the validity of the modeled $I(x)$ computed from Eq. (1). Through the experimental apparatus described in Ref. 31, simultaneous acquisitions of both the droplet signals and the video images have been performed generating droplets in the dripping to squeezing transition by fixing the flow rate $Q_D = 10\,\mu$L/min and changing Q_C in the range (see Ref. 25; 100 μL/min). The far dripping regime has been achieved at $Q_C = 100\,\mu$L/min, the transition regime at $Q_C = 50\,\mu$L/min, and the far squeezing regime at $Q_C = 25\,\mu$L/min. In Fig. 4, the considered droplet profiles $D(x)$ have been reported in function of x for comparison. In Figs. 5–7, the model predictions associated with such profiles are compared to the experimental signals and droplet images, as measured by the reference opto-microfluidics platform used in Refs. 13, 14, and 31.

In the squeezing regime (Fig. 5), the droplet fills the microfluidic channel, and, while flowing, it assumes a bullet shape with a frontal meniscus that is flatter than the posterior one, depending on the droplet velocity [see Fig. 5(a), camera image]. The light intensity detected by the output waveguide is reported as a function of the passage time [see Fig. 5(a), experimental signal]: primary intensity peaks are detected at the beginning and the end of the droplet (A), respectively, followed by a shoulder (S) and a plateau (T). When the droplet is obstructing the waveguide axis, $I(x)$ drops to the minimum value, corresponding to the case where the transmission predominates (T).

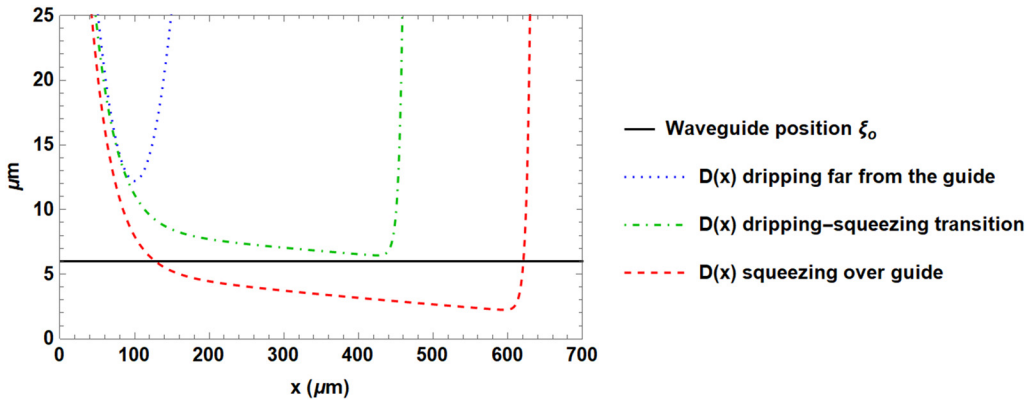

FIG. 4. $D(x)$ is reported in function of x. The waveguide position ξ_0 is also reported (6 μm in the simulation), to highlight when the droplet intersects the waveguide axis. All the three modeled profiles considered fulfill the detection condition set by the diffraction limit $D(x) < D_C$.

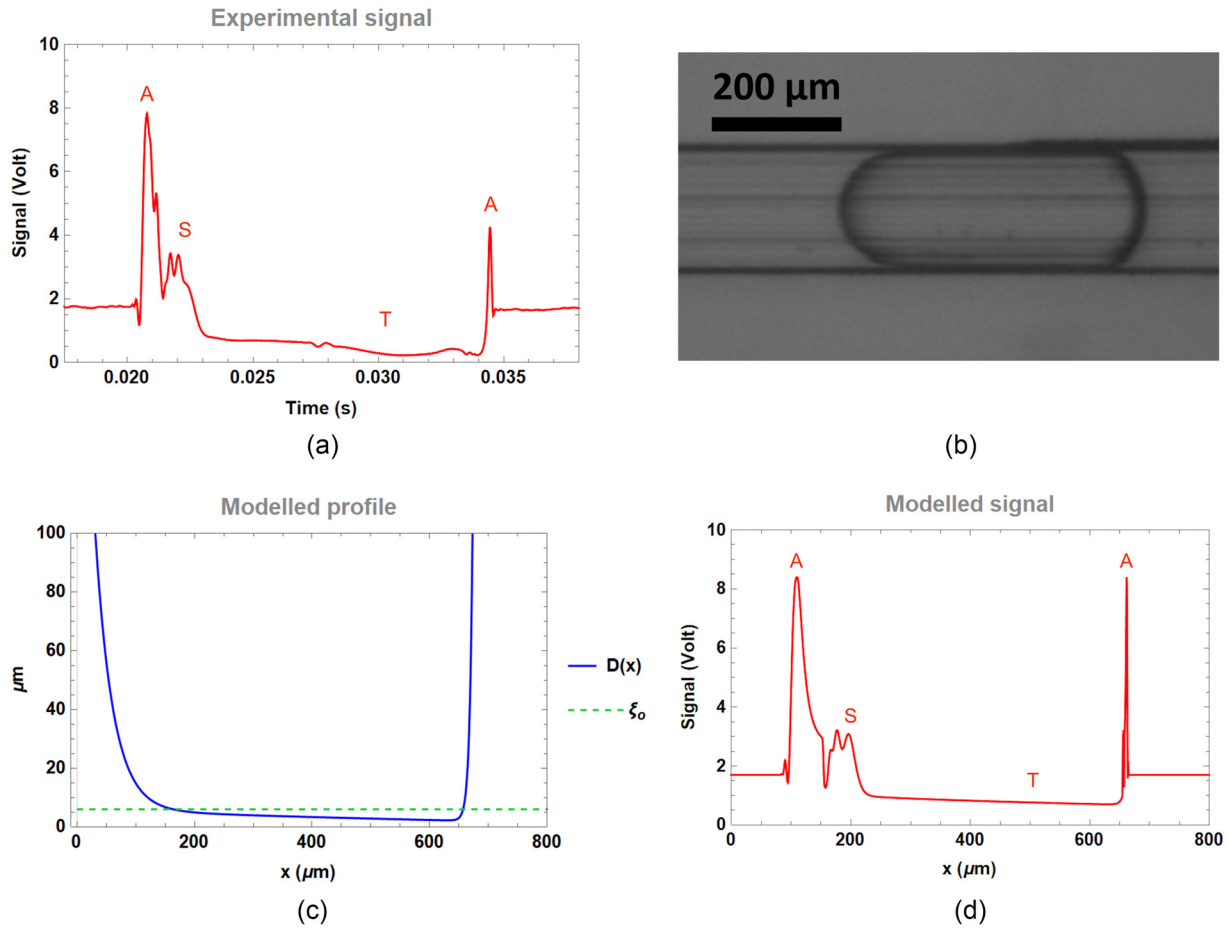

FIG. 5. (a) Experimental intensity measured by the reference device in the squeezing regime at $\lambda = 632.8$ nm and (b) an image of droplet acquired through a Basler acA800-510um camera placed below the reference device; (c) modeled profile $D(x)$ according to the video image, with $\xi_0 = 6$ μm the simulated position of the waveguide with respect to the microfluidic channel cover and (d) theoretically modeled signal (*Signal, [V]*) as predicted by Eq. (1) for $\lambda = 632.8$ nm.

The experimental D profile has been modeled with the equation reported in Fig. 5(b), and the relative modeled profile is, therefore, shown together with the resulting modeled signal $I(x)$. A decrease in $D(x)$ means that the droplet section is increasing in the channel: the model clearly shows that in this case, the contribute of $I(x)_{DIFF}$ plays a major role in justifying the presence of intensity peaks of the experimental droplet signal recorded at given geometrical conditions. In the configuration herein considered, it results that $D(x)|_{\max} = 12\ \mu$m and $D(x)|_{\min} \sim 17\ \mu$m, coherent with the predicted $D_C \approx 16\ \mu$m and lying in the transition region considered in $f(x)_{DIFF}$. Diffraction minima determine the beginning and the ending of the signal according to the definition of transit time of the droplet within the light cone and clearly identifying the associated droplet signal. On the other hand, diffraction maxima account for intensity peaks as expected. Secondary peaks are always detected both in the model and in the experimental data at the beginning and the ending of the signal and mark the first and the last interaction between the droplet and the light cone, respectively. The model shows that such secondary peaks are generated again by diffraction. The shoulder (S) is due to the collimation effect [see δ in Eq. (11)], and the signal plateau T is due to the transmitted light (I_T, I_{T2}). With respect to the other regimes, only in the far squeezing, a fall in the signal intensity is registered in the central part of the signal, since the droplet intersects the waveguide axis, and the conditions of direct transmission ($D(x) < \xi_0$) are established. Such decrease is caused by both the decreasing diffraction and the low values of I_T because the direct rays are predicted to impact on the droplet surface at angles close to the critical one.

Both in the dripping-to-squeezing transition (Fig. 6) and in the far squeezing (Fig. 5), the diffraction divergence condition is overcome with two separate peaks that can be detected. However, in the transition regime, the model suggests that the plateau value is higher than both the background intensity I_{BG} and the far squeezing regime [see Figs. 6(a) and 6(b)] because of the greater role played by I_R and I_{DIFF} due to the collimation effect expressed with the function $\delta(x)$ in Eq. (11) [$D(x)$ being quite close to ξ_0].

Finally, in the dripping regime, the experimental signal [Fig. 7(a)] shows a single peak of $I(x)$ and two secondary peaks at the beginning and the end of the signal. The model shows that the presence of a

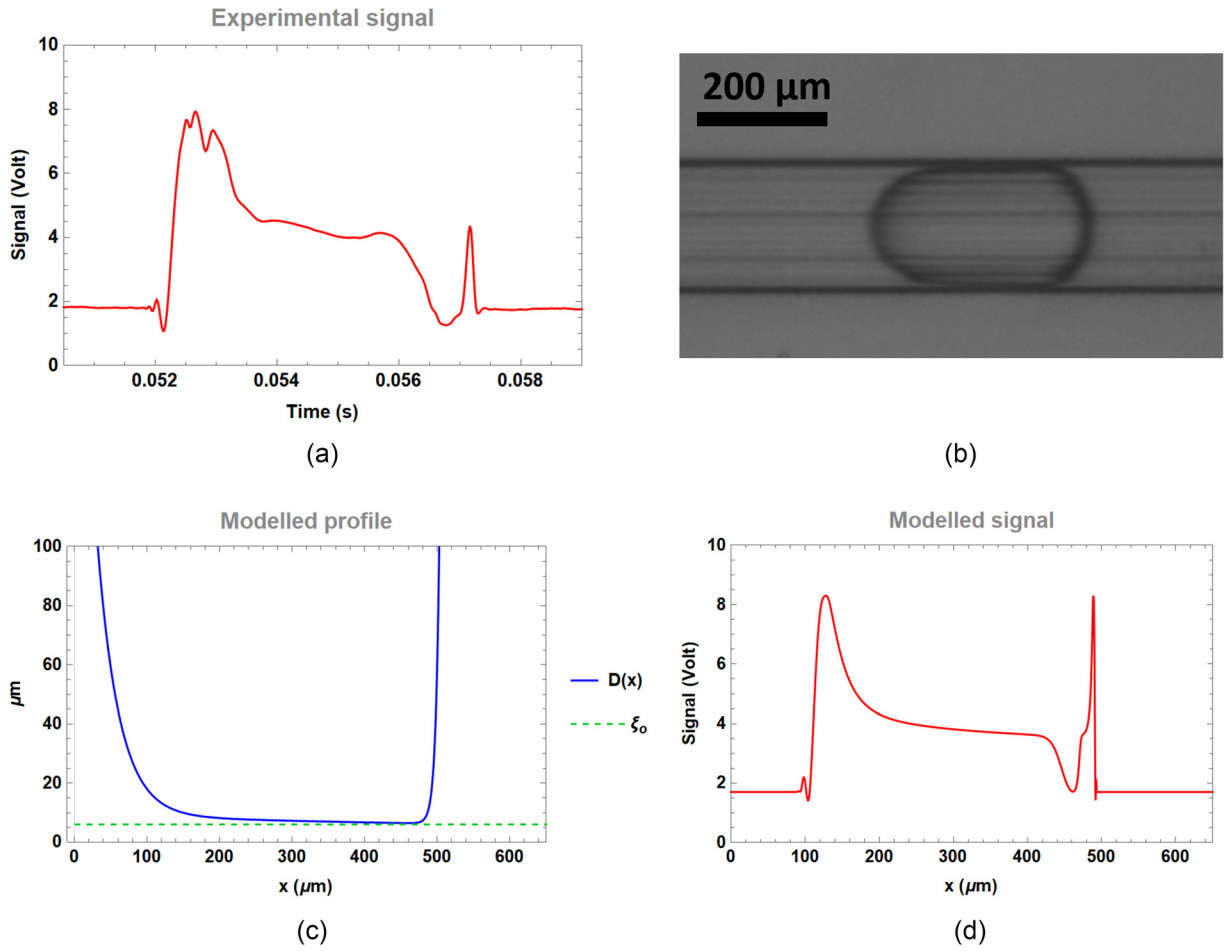

FIG. 6. (a) Experimental intensity measured by the reference device in the dripping-to-squeezing regime at $\lambda = 632.8$ nm and an (b) image of droplet acquired through a Basler acA800-510um camera placed below the reference device; (c) modeled profile $D(x)$ according to the video image, with $\xi_0 = 6\ \mu$m the simulated position of the waveguide with respect to the microfluidic channel cover and (d) theoretically modeled signal (*Signal, [V]*) as predicted by Eq. (1) for $\lambda = 632.8$ nm.

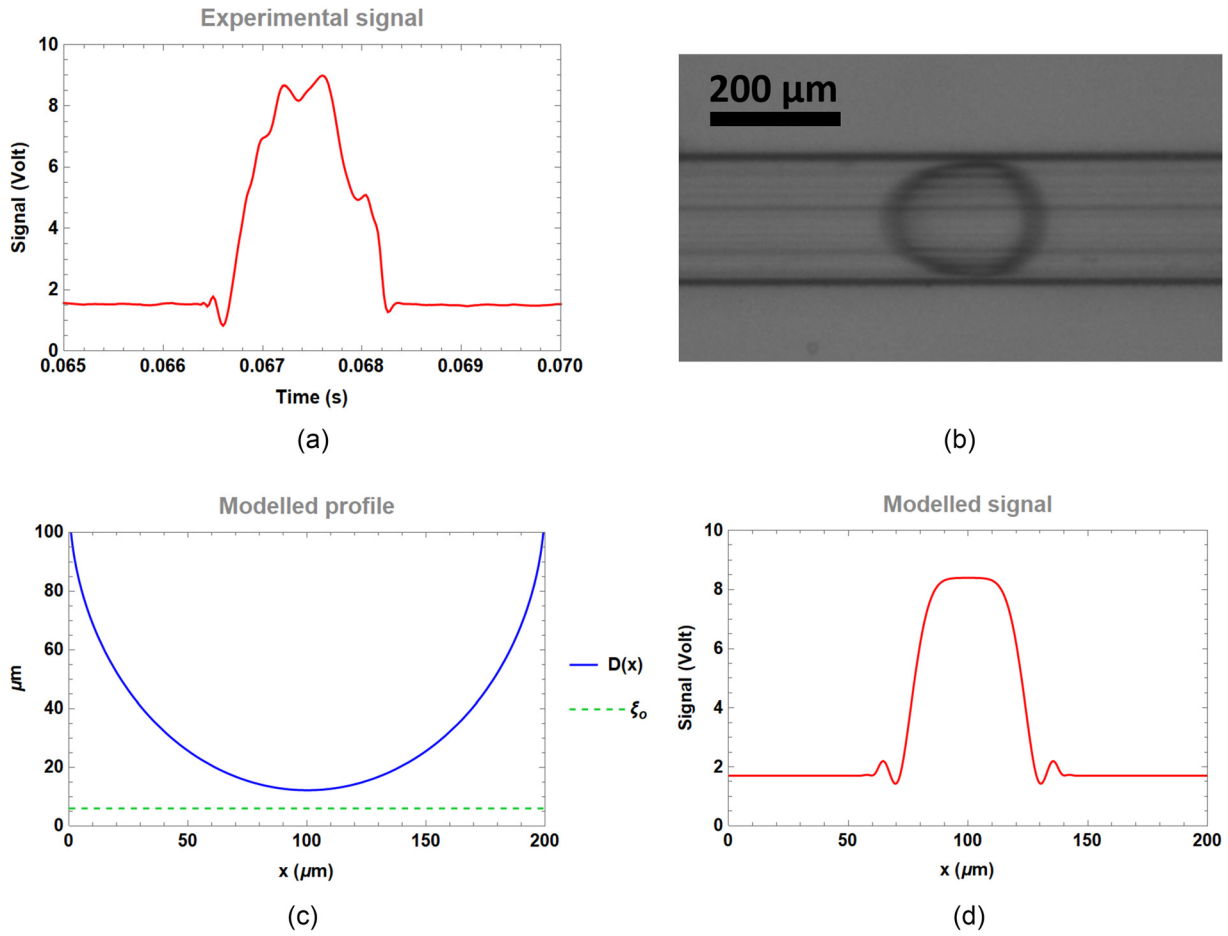

FIG. 7. (a) Experimental intensity measured by the reference device in the dripping regime at $\lambda = 632.8$ nm and (b) an image of droplet acquired through a Basler acA800-510um camera placed below the reference device; (c) modeled profile $D(x)$ according to the video image, with $\xi_0 = 6$ μm the simulated position of the waveguide with respect to the microfluidic channel cover and (d) theoretically modeled signal (*Signal, [V]*) as predicted by Eq. (1) for $\lambda = 632.8$ nm.

single peak in this case is due to the fact that $I(x)_T$, $I(x)_{T2}$, and $I(x)_{FC}$ herein vanish since $D(x)$ never crosses the waveguide position ξ_0, while I_{DIFF} and I_R predominate for $D(x) \geq D(x)|_{\max}$. As a consequence, a sort of lens effect can be detected at the output waveguide.

In conclusion, independently of the analyzed regime, strong intensity peaks are predicted near the divergence condition set by the diffraction at $D(x) = D(x)|_{\max}$. Moreover, in all the considered cases, the comparison between the modeled signals and the experimental acquisitions results in good agreement. Such agreement is set by focusing on the entire shape of the signals arising from the model and the experiment and not on their single values, thus exploiting the background intensity I_{BG} associated with the absence of the droplet as a voltage of normalization. In fact, such strategy is mandatory in studying this signal in order to get results independent from the light intensity coupled to the waveguide. In any case, by simply rescaling through a renormalization factor, the compared signals of Figs. 5–7 were all set at similar background intensities, just to ease the view and the comparison between model and experiment.

Focusing now on the weight of each contribute, the model allows to evaluate the origin of the structured shape of the transmission profile in a quantitative way. By plotting the I_i contributes for each microfluidic regime (see, for example, Fig. 8), it is possible to evidence their role and relative fingerprints in the signal as well as to quantify how much their relative weight is. In Table I, the impact and quantification of each contribute to the modeled $I(x)$ are summarized, reporting for each contribute the percentage of its integral over the integral of the whole signal, calculating both the integrals along all the signal time duration. In the squeezing regime, the phenomena depending on the light transmission play an important role, while in the dripping regime, physical phenomena depending on scattering and reflection effects are predominant. The model shows that only in the squeezing regimes, $I(x)_{T,FC}$ contributes significantly, as expected by the geometrical considerations.

Moreover, the role of the experimental conditions employed can be investigated and explained through the model as well. The change of the wavelength in the experimental acquisitions from $\lambda = 632.8$ nm to another value determines an impact on the signal that can be

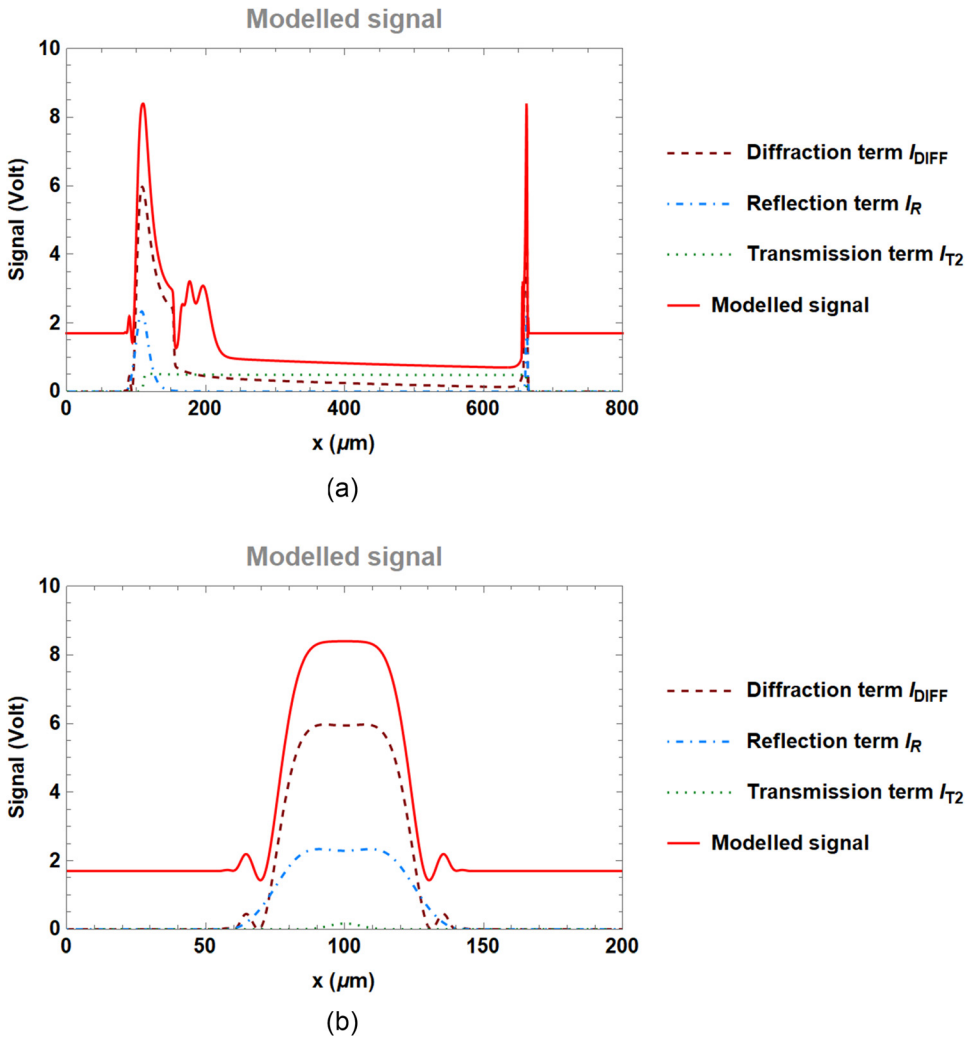

FIG. 8. Intensity $I(x)$ computed at the output waveguide and main contributes (I_i) for the squeezing (a) and dripping (b) regimes, compared to the modeled signal $I(x)$.

predicted according to the wavelength dependences in each I_i term. The diffused transmission component strongly depends on λ via the number of diffused rays $F_i(x, \lambda)$, since the geometrical conditions setting the diffusion depend on λ. By comparing the modeled signal to the experimental ones, it emerges that in average, several internal reflections are encountered and, in particular, $F_i(x) \sim 5$ at $\lambda = 632.8$ nm. In any case, due to the many optical components acting simultaneously, the dependence of the whole signal on λ is quite complex. Experimental data have been recorded also at $\lambda = 532$ nm, showing similar shapes in the experimental signals obtained at $\lambda = 632.8$ nm apart from a shrinking effect in the signal duration. The starting and ending points are set by the diffraction minima $D(x)_{\min}$ arising from I_{DIFF}, i.e., when $D(x)$ reaches the critical value D_C. The model herein proposed adequately explains this effect since it predicts that $D(x)_{\min}|_{\lambda=632\,\text{nm}} = 17.2\,\mu$m while $D(x)_{\min}|_{\lambda=532\,\text{nm}} = 16.5\,\mu$m. When $D(x)$ is decreasing (i.e., while the droplet section is increasing in the channel), red light ($\lambda = 632.8$ nm) induces diffraction before green light ($\lambda = 532$ nm) and so the transit time for $\lambda = 632.8$ nm is longer than the one for $\lambda = 532$ nm.

TABLE I. Impact and quantification of each contribute to the modeled $I(x)$ in function of the droplet profile $D(x)$ adopted. The minimum distance between the droplet top and the bottom cover in the simulated profile $D(x)$ is also reported for each configuration considered.

Droplet characteristics	Min$[D(x)]$ (μm)	$I(x)_{DIFF}$ (%)	$I(x)_R$(%)	$I(x)_T$(%)	$I(x)_{T2}$(%)	$I(x)_{FC}$(%)
Squeezing	2.2	42.7	6.7	5.7	34.5	10.5
Dripping-squeezing transition	6.5	82.3	5.5	0.0	12.2	0.0
Dripping	12.2	69.5	29.9	0.0	0.6	0.0

As far as the impact of the microfluidic channel is concerned, the modeled $I(x)$ predicts that increasing values of w correspond higher values of D_C as well as lower values of $I(x)$ because I_{DIFF} scales as w^{-3}; I_{BG} scales as w^{-2} and I_R scales as $e^{-w^{-2}}w^{-2}$. The model remains coherent in the phenomena description and is general enough to describe the light interaction with droplets flowing in a microfluidic channel, provided that the dispersed and continuous phases refractive indexes are considered. Although the theoretical derivation here detailed has considered the case $n_o > n_d$, the same approach can be used also for $n_o < n_d$. In the last case, in fact, in the reflection term $I_R(x)$, the reflectivity on the droplet top has to be considered, since the TIR condition is not satisfied anymore. The terms I_R, I_T, I_{T2}, F_C depend on the chosen geometrical configuration (such as the channel width w) and on the transmittance/reflection coefficients. As a consequence these terms are strongly impacted by the opposite refractive index contrast. Regarding the detection potentialities of the presented configuration, it has been shown that in the squeezing regime, the transmission components allow for content detection, with absorbance effects amplified in the adopted configuration due to the longer optical path experienced by the rays that contribute to I_{T2}, giving a boost in sensitivity related to absorbing content.[38] On the contrary, obstacle diffraction induced by the droplet passage generates marked peaks and intensity patterns clearly related to the droplet shape and profile. It has been shown both in the model and in the experimental data that these effects enhance the detection of objects transiting in the channel by a factor of 4 with respect to the absence of the droplet, giving a clear fingerprint on their shape characteristics.

IV. CONCLUSIONS

For the first time, the optical phenomena originating from the interaction of the light coming from an input optical waveguide illuminating a moving droplet into a microfluidic channel from its sidewall have been modeled. Their relative interplay has been considered, evidencing the specific contribute to the detected light intensity originating from reflection, transmission, absorbance, and diffraction, depending on the droplet position. The model has demonstrated to predict precisely and accurately all the fingerprints shown in the light intensity resulting from the light-droplet interaction also as a function of the light wavelength, microfluidic channel geometry, and the refractive index of the dispersed/continuous phases. Its validity has been tested in different microfluidic regimes such as squeezing, dripping, and the transition dripping-to-squeezing, by comparing the model predictions to experimental data obtained by a $LiNbO_3$ opto-microfluidic platform.

It emerged that the impact and quantification of each contribute to the modeled $I(x)$ can be estimated and in particular

- diffraction occurs due to the passage of the droplet that creates a slit between its surface top and the microfluidic channel cover. This effect introduces peaks in the detected intensity, fingerprints that can be used to estimate the droplet size and shape;
- when the moving droplet has a higher refractive index than the continuous phase, an enhancement in the detected intensity can be observed due to: (i) reflections from the droplet surface that increase the light intensity passing across this slit and (ii) transmitted rays that have experienced several internal reflections within the droplet. In the last case, absorbance effect is amplified due to the longer optical path experienced by these rays;
- in the squeezing regime, the phenomena depending on the light transmission play a primary role;
- in the dripping regime, physical phenomena depend mostly on scattering and reflection effects.

The model has allowed us to identify the best microfluidic configuration to have the higher detected intensity depending on the sensing functionality as well as the portion of the detected signal to analyze to get needed information:

(a) to estimate the droplets size, the positions of the diffraction minima are the best indicators;
(b) to investigate the droplets content, the most convenient configuration is to maximize both I_T and I_{T2} (i.e., $D(x) \leq \xi_0$, squeezing regime);
(c) for droplets counting, the best configuration is to maximize the effect of I_{DIFF} (i.e., $\xi_0 < D(x) < D_C$). In this case, the ratio between the maximum of such peaks and the background is at least around 4 giving a boost in marking the droplet transit in the channel.

The possibility of identifying the interplay of the optical phenomena occurring and quantifying them allows to reconstruct and monitor the droplet dynamics and analyze the optical response in detail, boosting for high precision optical sensing applications.

SUPPLEMENTARY MATERIAL

See the supplementary material for the mathematical derivation of the equations and details on the hypotheses and constrains the model is based on.

AUTHOR DECLARATIONS

Conflict of Interest

The authors have no conflicts to disclose.

Author Contributions

Leonardo Zanini: Conceptualization (equal); Data curation (equal); Formal analysis (equal); Investigation (equal); Methodology (equal); Visualization (equal); Writing – original draft (equal); Writing – review & editing (equal). **Cinzia Sada:** Conceptualization (equal); Investigation (equal); Methodology (equal); Project administration (equal); Supervision (equal); Validation (equal); Visualization (equal); Writing – original draft (equal); Writing – review & editing (equal).

DATA AVAILABILITY

The data that support the findings of this study are available from the corresponding author upon reasonable request.

REFERENCES

[1]F. Onofri and S. Barbosa, "Optical particle characterization," in *Laser Metrology in Fluid Mechanics*, edited by A. Boutier (John Wiley & Sons, Inc., 2012).
[2]R. Xu, "Light scattering: A review of particle characterization applications," Particuology **18**, 11 (2015).

[3]S. Han, Z. Sun, Z. Feng Tian, T. Lau, and G. Nathan, "Particle velocity measurement within a free-falling particle curtain using microscopic shadow velocimetry," Opt. Express **29**, 10923 (2021).
[4]D. J. White, "PSD measurement using the single particle optical sizing (SPOS) method," Geotechnique **53**(3), 317 (2003).
[5]C. Tropea, "Optical particle characterization in flows," Annu. Rev. Fluid Mech. **43**(1), 399 (2011).
[6]L. O. Narhi, Y. Jiang, S. Cao, K. Benedek, and D. Shnek, "A critical review of analytical methods for subvisible and visible particles," Curr. Pharm. Biotechnol. **10**(4), 373 (2009).
[7]G. Testa, G. Persichetti, P. M. Sarro, and R. Bernini, "A hybrid silicon-PDMS optofluidic platform for sensing applications," Biomed. Opt. Express **5**, 417 (2014).
[8]M. Yin, B. Huang, S. Gao, A. P. Zhang, and X. Ye, "Optical fiber LPG biosensor integrated microfluidic chip for ultrasensitive glucose detection," Biomed. Opt. Express **7**(5), 2067 (2016).
[9]R. Osellame, H. Hoekstra, G. Cerullo, and M. Pollnau, "Femtosecond laser microstructuring: an enabling tool for optofluidic lab-on-chips," Laser Photonics Rev. **5**, 442 (2011).
[10]L. Kelemen, L. Lepera, B. Horvath, P. Ormos, R. Osellame, and R. M. Vazquez, "Direct writing of optical microresonators in a lab-on-a-chip for label-free biosensing," Lab Chip **19**, 1985 (2019).
[11]S. Grilli, S. Coppola, G. Nasti, V. Vespini, G. Gentile, V. Ambrosio, C. Carfagna, and P. Ferraro, "Hybrid ferroelectric–polymer microfluidic device for dielectrophoretic self-assembling of nanoparticles," RSC Adv. **4**, 2851 (2014).
[12]S. Piacentini, F. Bragheri, G. Corrielli, R. M. Vázquez, P. Paiè, and R. Osellame, "Advanced photonic and optofluidic devices fabricated in glass via femtosecond laser micromachining," Opt. Mater. Express **12**, 3930 (2022).
[13]M. Chauvet, L. Al Fares, B. Guichardaz, F. Devaux, and S. Ballandras, "Integrated optofluidic index sensor based on self-trapped beams in $LiNbO_3$," Appl. Phys. Lett. **101**(1829), 181104 (2012).
[14]R. Zamboni, A. Zaltron, M. Chauvet, and C. Sada, "Real-time precise microfluidic droplets label-sequencing combined in a velocity detection sensor," Sci. Rep. **11**, 17987 (2021).
[15]G. Bettella, R. Zamboni, G. Pozza, A. Zaltron, C. Montevecchi, M. Pierno, G. Mistura, C. Sada, L. Gauthier-Manuel, and M. Chauvet, "$LiNbO_3$ integrated system for opto-microfluidic sensing," Sens. Actuators B **282**, 391 (2019).
[16]A. L. Aden, "Scattering of electromagnetic waves from two concentric spheres," J. Appl. Phys. **22**, 1242 (1951).
[17]W. J. Glantschnig and S.-H. Chen, "Light scattering from water droplets in the geometrical optics approximation," Appl. Opt. **20**, 2499 (1981).
[18]J. Gebhart, "Response of single-particle optical counters to particles of irregular shape," Part. Part. Syst. Charact. **8**(1–4), 40 (1991).
[19]B. Wessely, S. Gabsch, J. Altmann, and F. Babick, "Single particle detection and size analysis with statistical methods from particle imaging data," Part. Part. Syst. Charact. **23**, 165 (2006).
[20]G. Gouesbet and G. Gréhan, *Optical Particle Sizing* (Springer, New York, 1988), p. XII, 642.
[21]F. Onofri, G. Gréhan, and G. Gouesbet, "Electromagnetic scattering from a multilayered sphere located in an arbitrary beam," Appl. Opt. **34**, 7113 (1995).
[22]B. Tolla and D. Boldridge, "Distortion of single-particle optical sensing (SPOS) particle count by sub-countable particles," Part. Part. Syst. Charact. **27**, 21 (2010).
[23]A. J. Bale, "*In situ* laser optical particle sizing," J. Sea Res. **36**(1–2), 31 (1996).
[24]M. Chen, Y. Wang, W. Li, M. Xia, Z. Meng, and L. Xia, "A Dual-angle fiber dynamic light scattering system integrated with microfluidic chip for particle size measurement," Opt. Laser Technol. **150**, 107891 (2022).
[25]F. Peng, L. K. Månsson, S. H. Holm, S. Ghosh, G. Carlström, J. J. Crassous, P. Schurtenberger, and J. O. Tegenfeld, "A droplet-based microfluidics route to temperature-responsive colloidal molecules," J. Phys. Chem. B **123**(43), 9260 (2019).
[26]F. R. A. Onofri, I. Rodriguez-Ruiz, and F. Lamadie, "Microfluidic lab-on-a-chip characterization of nano- to microparticles suspensions by light extinction spectrometry," Opt. Express **30**, 2981 (2022).
[27]Q. Li, H. Huang, F. Lin, and X. Wu, "Optical micro-particle size detection by phase-generated carrier demodulation," Opt. Express **24**, 11458 (2016).
[28]M. P. Sentis, F. R. Onofri, L. Méès, and J. St. Radev, "Scattering of light by large bubbles: Coupling of geometrical and physical optics approximations," J. Quant. Spectrosc. Radiat. Transfer **170**, 8 (2016).
[29]L. Li, P. G. Stegmann, S. Rosenkranz, W. Schäfer, and C. Tropea, "Simulation of light scattering from a colloidal droplet using a polarized Monte Carlo method: Application to the time-shift technique," Opt. Express **27**, 36388 (2019).
[30]F. Jaillon and H. Saint-Jalmes, "Description and time reduction of a Monte Carlo code to simulate propagation of polarized light through scattering media," Appl. Opt. **42**(16), 3290 (2003).
[31]L. Zanini, A. Zaltron, E. Turato, R. Zamboni, and C. Sada, "Opto-microfluidic integration of the bradford protein assay in lithium niobate lab-on-a-chip," Sensors **22**(3), 1144 (2022).
[32]L. Shang, Y. Cheng, and Y. Zhao, "Emerging droplet microfluidics," Chem. Rev. **117**(12), 7964 (2017).
[33]Y. Ding, P. D. Howes, and A. J. DeMello, "Recent advances in droplet microfluidics," Anal. Chem. **92**(1), 132 (2020).
[34]P. Guillot, A. Ajdari, J. Goyon, M. Joanicot, and A. Colin, "Droplets and jets in microfluidic devices," C. R. Chim. **12**(1–2), 247 (2009).
[35]S. Nizamov, S. D. Sazdovska, and V. M. Mirsky, "A review of optical methods for ultrasensitive detection and characterization of nanoparticles in liquid media with a focus on the wide field surface plasmon microscopy," Anal. Chim. Acta **1204**, 339633 (2022).
[36]J. T. Butement, H. C. Hunt, D. J. Rowe, N. P. Sessions, O. Clark, P. Hua, G. Senthil Murugan, J. E. Chad, and J. S. Wilkinson, "Integrated optical waveguides and inertial focussing microfluidics in silica for microflow cytometry applications," J. Micromech. Microeng. **26**, 105004 (2016).
[37]N. T. Nguyen, S. Lassemono, and F. A. Chollet, "Optical detection for droplet size control in microfluidic droplet-based analysis systems," Sens. Actuators B **117**(2), 431 (2006).
[38]L. Zanini, A. Zaltron, R. Zamboni, E. Turato, and C. Sada, "Enhanced sensing to characterize microdroplets through induced optical phenomena in integrated opto-microfluidic lab-on-a-chip," SPIE Opt. Sens. Detect. VII **12139**, 106 (2022).